Transport Properties of Hybrid Zigzag Graphene and Boron Nitride Nanoribbons

ARTICLE *in* THE JOURNAL OF PHYSICAL CHEMISTRY C · MAY 2011

Impact Factor: 4.77 · DOI: 10.1021/jp200870t

THE JOURNAL OF PHYSICAL CHEMISTRY C

ARTICLE

pubs.acs.org/JPCC

Transport Properties of Hybrid Zigzag Graphene and Boron Nitride Nanoribbons

Zhizhou Yu, M. L. Hu, C. X. Zhang, C. Y. He, L. Z. Sun,* and Jianxin Zhong*

Laboratory for Quantum Engineering and Micro-Nano Energy Technology, Xiangtan University, Xiangtan 411105, China

Supporting Information

ABSTRACT: The transport properties of hybrid nanoribbons formed by partially substituting zigzag boron nitride (graphene) nanoribbons into zigzag graphene (boron nitride) nanoribbons are investigated using the first-principles nonequilibrium Green's function method. The transport properties are highly improved with the transmission conductance around the Fermi level increasing to $3G_0$ in hybrid systems based on zigzag graphene nanoribbons and to $2G_0$ in hybrid systems based on zigzag boron nitride nanoribbons. The enhancement is attributed to the coupling effect between B (N) atoms and C atoms at the interface of hybrid systems, which introduces a pair of bonding and antibonding bands around the Fermi level. The transport enhancement also remains in hybrid nanoribbons sandwiched into gold electrodes. The currents of such devices are improved compared with those of pristine ones, which originate from the additional transport channels at the C−B interface.

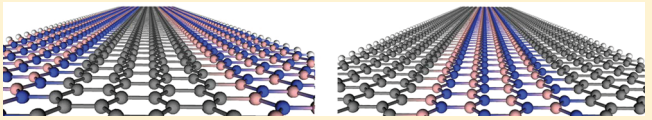

INTRODUCTION

Graphene, a single layer of carbon atoms arranged in a hexagonal lattice, attracts great interest as a fascinating material in nanoelectronics due to its unique electronic structures and transport properties.[1,2] Moreover, graphene nanoribbons (GNRs),[3] quasi-one-dimensional materials patterned from graphene, have been predicted to be a promising candidate in future carbon-based electronics. Lots of prototypic devices, such as field effect transistors,[4] have been fabricated by GNRs. Recently, monolayer and multilayer boron nitride sheets have been successfully prepared in experiments.[5−7] Analogously, boron nitride nanoribbons (BNNRs) draw a great deal of attention due to their potential applications in optics and opto-electronics. Unlike GNRs, BNNRs are wide gap semiconductors whose electronic properties are much less dependent on their chirality and geometry.[8−10] However, the electronic properties of GNRs and BNNRs can be effectively modulated by chemical decoration and defects.[11−13]

Subsequent to the discovery of GNRs and BNNRs, the hybrid systems of GNRs and BNNRs attract increasing interest due to their novel electronic properties and potential applications in nanotechnology. The tunable bandgap is shown in hybrid nanotubes rolling from GNRs and BNNRs by ab initio calculations.[14] Moreover, theoretical results not only prove the stability of such hybrid structures but also show half-metallic behavior in some GNRs−BNNRs hybrid systems with different edge shapes.[15−18] The hybrid structure will offer us an effective approach to modulate the electronic properties of BNNRs and GNRs. By modulating the site potential, Semenoff et al.[19] introduce an interesting domain wall into gapped GNRs which behaves as a metallic quantum wire. The GNRs−BNNRs hybrid structure offers the possibility to achieve such a domain in GNRs and BNNRs practically. Using the first-principles method coupled with the nonequilibrium Green's function, we explore the transport properties of hybrid nanoribbons formed by partially substituting zigzag BNNRs (ZBNNRs) into zigzag GNRs (ZGNRs) and partially substituting ZGNRs into ZBNNRs. The transport properties of hybrid structures are highly improved compared with those of pristine ones. The transmission conductance around the Fermi level of ZGNR-based and ZBNNR-based hybrid systems increases to $3G_0$ and $2G_0$, respectively. The enhancement is attributed to the coupling effects between B (N) atoms and C atoms at the interfaces of hybrid systems. Moreover, the transport enhancement remains in the hybrid nanoribbons combined with gold electrodes. The currents of Au|hybrid nanoribbons|Au are improved compared with those of pristine nanoribbons due to the additional transport channels introduced by C−B interfaces in these systems.

COMPUTATIONAL METHODS

To investigate the structural and electronic properties of hybrid nanoribbons, we adopt the Vienna Ab initio Simulation Package (VASP) to perform the first-principles plane-wave calculations within the density functional theory (DFT).[20,21] We choose the projector augmented wave (PAW) potentials to describe the electron−ionic core interaction. The exchange and correlation are approximated by generalized gradient approximation (GGA) with the Perdew−Burke−Ernzerhof (PBE) functional.[22] A plane-wave basis set with the kinetic energy cutoff of 450 eV is employed. Atoms are relaxed with the residual force less than 0.02 eV/Å, and the total energies are converged to 10^{-5} eV. The Atomistix ToolKit (ATK) implementation, using the

Received: January 27, 2011
Revised: March 31, 2011
Published: May 06, 2011

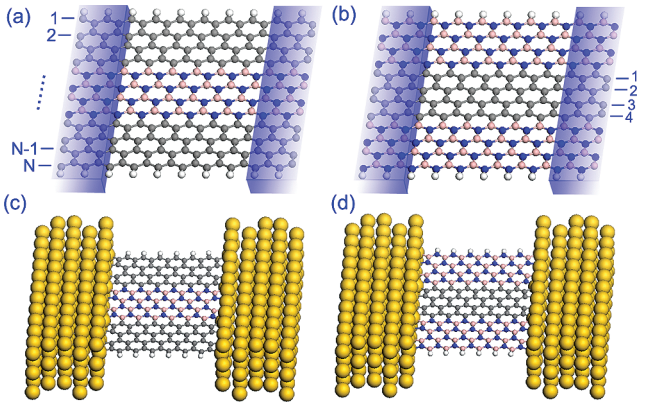

Figure 1. Schematic diagram of the device constructed by hybrid systems of 4-ZBNNR/ZGNR (a) and 4-ZGNR/ZBNNR (b). The light blue shadows represent the electrodes. Two-probe devices constructed by 4-ZBNNR/ZGNR (c) and 4-ZGNR/ZBNNR (d) sandwiched into Au(111)-3 × 12 electrodes. The white, pink, gray, blue, and golden balls denote the hydrogen, boron, carbon, nitrogen, and gold atoms, respectively.

first-principles method combined with the nonequilibrium Green's function, is used for transport calculations.[23] The double-plus ζ polarization numerical orbital basis set is chosen for boron, carbon, and nitrogen atoms. The exchange and correlation potentials are also approximated by GGA with PBE functional.[22] The mesh cutoff is set to be 150 Ry, and the convergence of total energies is set to be 10^{-5} Ry. As for systems with gold electrodes, the single-plus ζ polarization numerical orbital basis set is chosen for gold atoms, and the mesh cutoff is set to be 250 Ry. All computational parameters used in our present work are optimized.

We test the compatibility of the combination of the two different methods. The transmission spectra of ZGNRs relaxed by either VASP or ATK show the same characteristics. Thus, we combine the efficient aspect of both methods, namely, using VASP to relax the structures and ATK to obtain their transport properties. The transmission properties of ZGNRs with different length within gold electrodes are also tested. The transmission conductance of Au|ZGNR|Au shows similar characteristics around the Fermi level when the length of ZGNR is larger than 6.5 unit cells (the comparison of the transmission conductance between 6.5 and 12.5 unit cells is shown in the Supporting Information, Figure S1). Therefore, we sandwich hybrid nanoribbons of 6.5 unit cells into gold electrodes to construct our proposed devices. According to previous studies,[17,24] the energy of the spin-polarized state of ZGNRs, ZBNNRs, and typical hybrid ZGNRs−ZBNNRs systems is around 30 meV per unit cell lower than that of the spin-unpolarized state. The energy is too small to stabilize the spin-polarized state which would become unstable at finite temperature or in the presence of a ballistic current through the device.[24,25] To show the detectable transport properties in experiments, we just consider the spin-unpolarized state in our present study.

RESULTS AND DISCUSSION

The widths of ZGNRs and ZBNNRs are denoted by the number of zigzag chains, as shown in Figure 1. We substitute ZBNNRs with different widths into 12-ZGNR and substitute ZGNRs with different widths into 12-ZBNNR to construct the hybrid structures. We refer to the two hybrid structures as Ns-ZBNNR/ZGNR and Ns-ZGNR/ZBNNR, where Ns is the ribbon width of the substituted ZBNNR and the substituted ZGNR, respectively. 4-ZBNNR/ZGNR and 4-ZGNR/ZBNNR are presented in Figure 1(a) and Figure 1(b), respectively. All hybrid structures are fully relaxed. The same structures are used for semi-infinite electrodes to exclude the influence of heteroelectrodes. To evaluate the stability of different hybrid systems, the Gibbs free energy of formation δG is used, which is defined as[26]

$$\delta G = E(\text{tot}) - \chi_H\mu_H - \chi_C\mu_C - \chi_{BN}\mu_{BN} \quad (1)$$

where E(tot) is the cohesive energy per atom of the hybrid nanoribbon with different compositions; χ_i is the molar fraction of atom i (i = H, C, BN) in the structure satisfying $\chi_H + \chi_C + \chi_{BN} = 1$; and μ_i is the chemical potential of each constituent atoms. We choose μ_H as the binding energy per atom of the H_2 molecule and μ_C and μ_{BN} as the cohesive energies per atom of a single-layer graphene sheet and BN sheet, respectively. Our calculated δG is less than 85 meV/atom for all hybrid structures, which is as stable as the C/BN hybrid zigzag nanoribbons reported in previous work.[17] Moreover, it is an exothermic reaction in forming the hybrid systems from ZBNNRs and ZGNRs.

Figure 2(a) presents the transmission spectra of ZGNR-based hybrid systems and that of the pristine ZGNR for comparison. As for the pristine ZGNR, the transmission conductance is about $1G_0$ within the energy window of (−0.85, 0.85) eV, which is the limit to achieve the ballistic transport. A peak of $3G_0$ appears at the Fermi level which derives from the flat band, and the detailed discussions can be found in ref 27. As for 1-ZBNNR/ZGNR, the transmission spectrum is similar to that of the pristine ZGNR around the Fermi level. However, the transmission conductance increases from $1G_0$ to $3G_0$ in the energy windows of (−0.55, −0.4) eV and (0.4, 0.55) eV due to the substitution of ZBNNR into ZGNR. As the ribbon width of the substituted ZBNNR increases, the two $3G_0$ platforms approach the Fermi level, and they start to overlap when the ribbon width of ZBNNR exceeds 2. Moreover, the $3G_0$ peak of the pristine ZGNR and 1-ZBNNR/ZGNR at the Fermi level disappears as the ribbon width of ZBNNR increases to 2 because the flat band is affected by the substitution. As for 3-ZBNNR/ZGNR and 4-ZBNNR/ZGNR, the two $3G_0$ platforms overlap and introduce the high transmission conductance regions of (−0.2, 0.15) eV and (−0.15, 0.15) eV around the Fermi level, respectively. Thus, the transport properties of hybrid systems based on ZGNRs are significantly improved compared with those of pristine ZGNRs. However, as for 5-ZBNNR/ZGNR, those two platforms around the Fermi level start to separate each other. When the ribbon widths of ZBNNR increase further, the transmission conductance reduces to $1G_0$ at the Fermi level. Furthermore, the transmission spectrum of 9-ZBNNR/ZGNR and 10-ZBNNR/ZGNR exhibits a dip of $0G_0$ and a small transmission gap of 0.05 eV around the Fermi level, respectively.

The transmission spectra of ZBNNR-based hybrid systems are presented in Figure 2(b), and that of the pristine ZBNNR is also included for comparison. There is a large transmission gap about 4 eV around the Fermi level for the pristine ZBNNR due to its semiconducting characteristics. As for 1-ZGNR/ZBNNR, 2-ZGNR/ZBNNR, and 3-ZGNR/ZBNNR, the transmission gap reduces to 1.55, 0.5, and 0.05 eV, respectively. When the ribbon width of the substituted ZGNR increases to 2, a peak of $2G_0$ occurs at each side of the transmission gap (around ±0.3 eV). These two peaks approach the Fermi level and then overlap

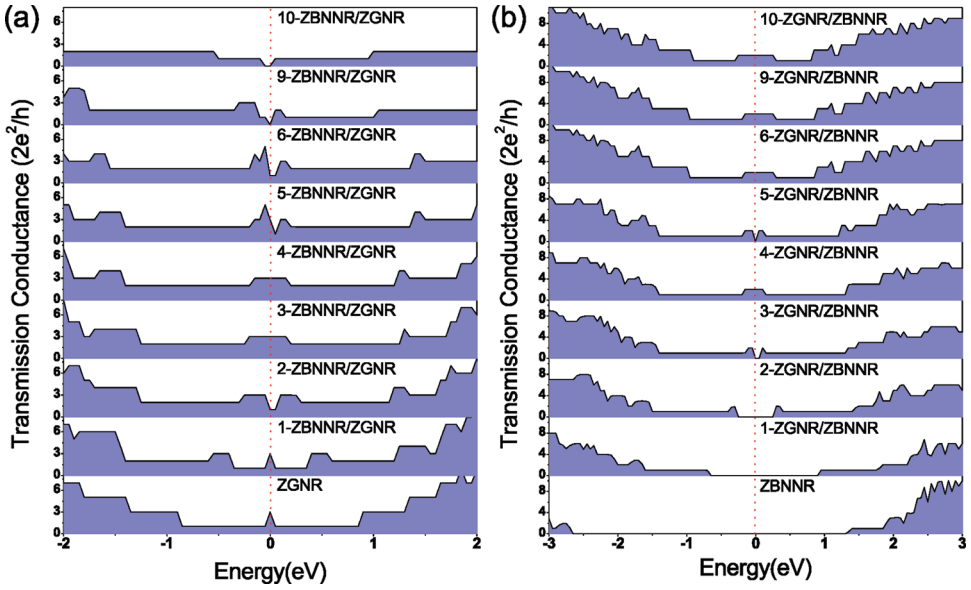

Figure 2. (a) Transmission spectra of Ns-ZBNNR/ZGNR and the pristine ZGNR. (b) Transmission spectra of Ns-ZGNR/ZBNNR and the pristine ZBNNR.

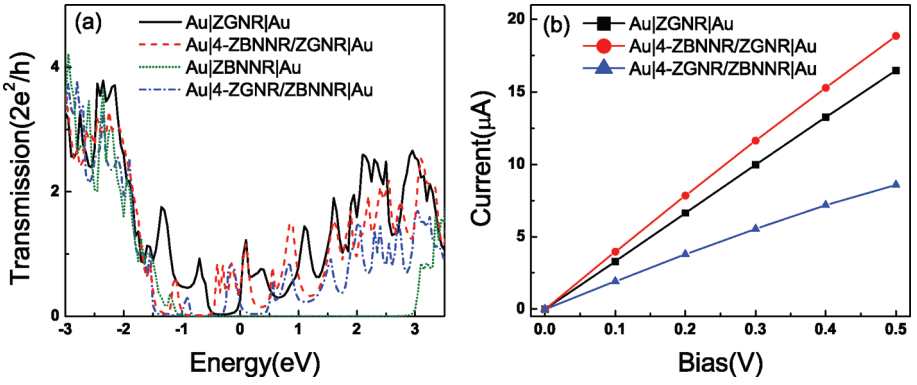

Figure 3. (a) Transmission spectra of Au|ZGNR|Au, Au|4-ZBNNR/ZGNR|Au, Au|ZBNNR|Au, and Au|4-ZGNR/ZBNNR|Au. (b) $I-V$ curves of Au|ZGNR|Au, Au|4-ZBNNR/ZGNR|Au, and Au|4-ZGNR/ZBNNR|Au.

at the Fermi level, spanning the energy window of $(-0.15, 0.1)$ eV for 4-ZGNR/ZBNNR. Hence, the transmission conductance shows metallic characteristics, which reveal that the transport properties of hybrid systems based on ZBNNRs are notably enhanced compared with those of pristine ZBNNRs. As the ribbon width of the substituted ZGNR increases further, the $2G_0$ platform remains around the Fermi level, and its energy span increases to 0.4 and 0.5 eV for 9-ZGNR/ZBNNR and 10-ZGNR/ZBNNR, respectively. Our results imply that the modulation of the transmission conductance of hybrid ZGNRs−ZBNNRs systems is dependent on the concentration of substituted nanoribbons.

We then calculate their transport properties within metal electrodes because nanoribbons are always combined with metal electrodes in applications. We choose two typical hybrid systems, 4-ZBNNR/ZGNR and 4-ZGNR/ZBNNR, and sandwich them into two semi-infinite Au(111) electrodes to construct our prototypic devices, as shown in Figure 1(c) and Figure 1(d), respectively. The pristine ZGNR and ZBNNR with the same width of hybrid systems are also sandwiched into gold electrodes for comparison. The interfaces between the Au(111) surface and nanoribbons are fully relaxed. The transmission spectra are shown in Figure 3(a). There is a transmission peak around the Fermi level for Au|ZGNR|Au deriving from its edge states. As for Au|4-ZBNNR/ZGNR|Au, the peak mentioned above remains around the Fermi level, and three additional peaks occur below the Fermi level, which greatly enhance the total transmission around the Fermi level, especially in the energy window of $(-0.5, 0)$ eV. As for Au|ZBNNR|Au, the transmission spectrum shows a large transmission gap about 3.85 eV. Amazingly, a transmission peak occurs below the Fermi level for Au|4-ZGNR/ZBNNR|Au, which shows a transition from semiconductor to metal in the hybrid ZBNNRs. The $I-V$ characteristics are analyzed to further evaluate the transport enhancement under a certain bias, as shown in Figure 3(b). The $I-V$ curves are well linear for these two typical hybrid systems and pristine ZGNRs. The currents of Au|4-ZBNNR/ZGNR|Au are notably larger than those of Au|ZGNR|Au. We then get the conductance by linearly fitting the $I-V$ curves to quantify the enhancement. Our results show that the conductance of Au|4-ZBNNR/ZGNR|Au increases by

dx.doi.org/10.1021/jp200870t |J. Phys. Chem. C 2011, 115, 10836–10841

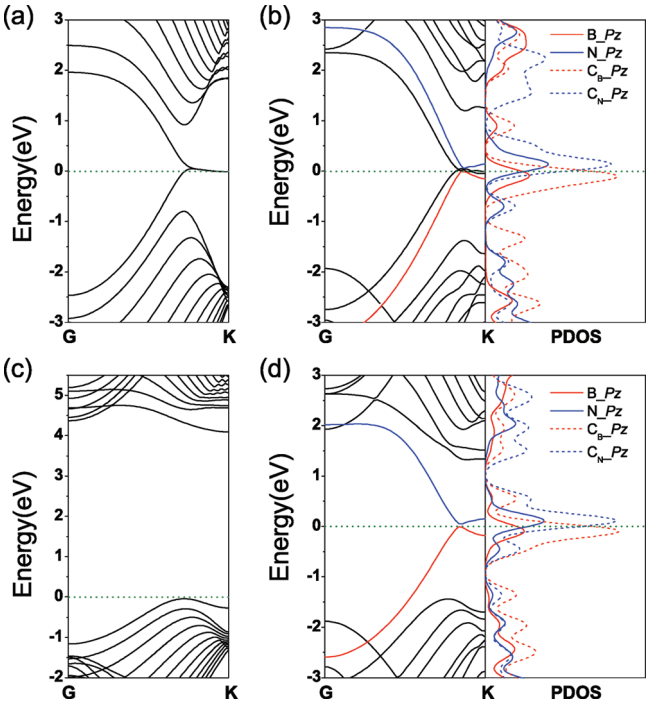

Figure 4. (a) Band structures of pristine ZGNR, (b) band structure and PDOS of 4-ZBNNR/ZGNR, (c) band structure of pristine ZBNNR, and (d) band structure and PDOS of 4-ZGNR/ZBNNR. B, N, C_B, and C_N represent the B and N atoms at the interfaces of hybrid systems and their interfacial C atoms, respectively.

about 15% compared with that of Au|ZGNR|Au, which indicates that hybrid ZGNRs exhibit better transport properties than the pristine one. As for Au|4-ZGNR/ZBNNR|Au, the conductance is about 54% of that of Au|ZGNR|Au, which obviously shows metallic characteristics. As we know, the $I-V$ curves of Au|ZBNNR|Au would exhibit a large threshold voltage. Our results indicate that the transport properties of hybrid ZBNNR systems are significantly enhanced.

To find out the reason for the enhancement of transport properties, we analyze their band structures and projected density of states (PDOS), as shown in Figure 4. The highest occupied valence band (HOVB) and the lowest unoccupied conduction band (LUCB) of the pristine ZGNR, as shown in Figure 4(a), are degenerate at the Fermi level and form the flat bands, which originate from the edge C atoms. As for 4-ZBNNR/ZGNR, the flat bands remain at the Fermi level though they are not as strictly degenerate and flat as those of the pristine ZGNR. Moreover, there is an extra band at each side of the Fermi level, namely, the second LUCB and the second HOVB, as shown in Figure 4(b). The PDOS indicates that the second LUCB derives from the hybridization between p_z states of N atoms at the interface and their nearest C atoms. However, the second HOVB derives from the hybridization between p_z states of B atoms at the interface and their nearest C atoms. These two bands show a strong mixing of π orbitals. The characteristics of such band structures are similar to that of the $C_{0.5}(BN)_{0.5}$ hybrid nanotube.[14] The bonding between C and N atoms at the C−N interface results in a higher antibonding orbital, which introduces a conduction band above the Fermi level. Similarly, the interaction of π orbitals at the C−B interface results in a lower bonding orbital, which introduces a valence band under the Fermi level. The density of states (DOS) around the Fermi level is greatly increased, and additional transport channels are introduced into the hybrid structure, by which the $3G_0$ transmission platform is introduced into each side of the Fermi level instead of $1G_0$ of the pristine ZGNR, as shown in Figure 2(a). The transmission conductance of $3G_0$ derives from the coupling between C and B (N) atoms at the interface and edge states of hybrid systems. These two bands approach the Fermi level for 4-ZBNNR/ZGNR, which leads to the overlap of two $3G_0$ transmission platforms around the Fermi level, as shown in Figure 2(a). Moreover, additional transmission peaks are introduced around the Fermi level for Au|4-ZBNNR/ZGNR|Au as shown in Figure 3(a) due to these additional transport channels. The transmission conductance is greatly enhanced in the energy window of (−0.5, 0) eV around the Fermi level compared with that of Au|ZGNR|Au of the same width. As for the pristine ZBNNR, the band structures show a wide gap of 4.36 eV as shown in Figure 4(c). The HOVB and LUCB originate from p_z states of edge N and B atoms, respectively. However, as for 4-ZGNR/ZBNNR, the HOVB (LUCB) mainly derives from the hybridization between p_z states of C atoms at the interface and their nearest B (N) atoms, as shown in Figure 3(d). The strong mixing of π orbitals between C and B (N) atoms at the interface shows characteristics similar to that of 4-ZBNNR/ZGNR. We find that the approach of HOVB and LUCB to the Fermi level reduces the bandgap of the hybrid ZBNNR and significantly increases the DOS around the Fermi level. Thus, the $2G_0$ transmission peak originating from the coupling between C and B (N) atoms at the interface is introduced into each side of the Fermi level, and they overlap and form a platform around the Fermi level as shown in Figure 2(b). A transmission peak is also introduced around the Fermi level for Au|4-ZGNR/ZBNNR|Au as shown in Figure 3(a), which leads to the enhanced transmission conductance compared with the pristine ZBNNR. Our results of the enhanced transport properties of hybrid ZGNRs−ZBNNRs systems indicate that the hybrid ZGNRs−ZBNNRs structure is an effective and efficient way to modulate the transport properties of GNR- and BNNR-based nanoelectronic devices.

As mentioned above, the transmission conductance modulation of hybrid systems is dependent on the concentration of substituted nanoribbons. To further clarify such dependence, we analyze the evolution of the energy gap (Δ) between the second HOVB and the second LUCB of ZGNR-based hybrid systems and the bandgap of ZBNNR-based hybrid systems as a function of the ribbon width of substituted nanoribbons, as shown in Figure 5. Δ reduces as the ribbon width of ZBNNR increases in hybrid systems initially, and Δ of 4-ZBNNR/ZGNR reduces to 61 meV. The decrease of Δ results in the enhancement of total DOS around the Fermi level and improves the transmission conductance of hybrid systems. However, Δ starts to increase when the width of substituted ZBNNR increases to 5 because the second HOVB and the second LUCB separate each other, which results in the separation of two $3G_0$ transmission platforms and less transport enhancement, as shown in Figure 2(a). The bandgap of ZBNNR-based hybrid systems decreases along with the increase in the ribbon width of substituted ZGNR until Ns exceeds 8. However, the bandgap of 9-ZGNR/ZBNNR and 10-ZGNR/ZBNNR is still very small (lower than 50 meV). It implies that the transport properties of ZBNNR-based hybrid systems are less dependent on the concentration of substituted nanoribbons than those of ZGNR-based hybrid systems.

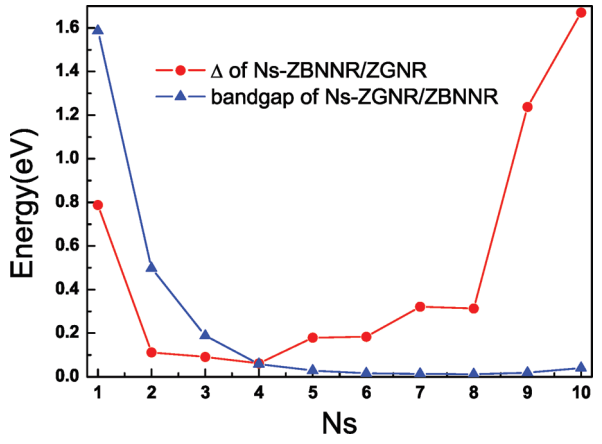

Figure 5. Energy gap Δ of Ns-ZBNNR/ZGNR and bandgap of Ns-ZGNR/ZBNNR as a function of the ribbon width of substituted nanoribbons. Δ is the energy gap between the second HOVB and the second LUCB of Ns-ZBNNR/ZGNR.

To illustrate the mechanism of the transport enhancement of hybrid systems within gold electrodes, we calculate the local density of states (LDOS) in the real space of Au|hybrid nanoribbons|Au. Figure 6(a) and Figure 6(b) show the LDOS at the Fermi level of Au|4-ZBNNR/ZGNR|Au and Au|4-ZGNR/ZBNNR|Au, respectively. The results indicate that the LDOS mainly distributes along with the edge C atoms and C−B interface of Au|4-ZBNNR/ZGNR|Au. As for Au|4-ZGNR/ZBNNR|Au, the LDOS mainly distributes along with the C−B interface. It means that the C−B interface introduced by substituted nanoribbons offers extra transport channels in hybrid systems, which enhances their transport properties. However, the C−N interface which introduces a conduction band around the Fermi level in hybrid nanoribbons does not behave as effective transport channels. To reveal such a phenomenon, we calculate the effective potential distribution between the Au(111) surface and C−B (C−N) interface of these two typical hybrid systems. The barrier between the Au(111) surface and C−N interface is 1.7 eV higher than that between the Au(111) surface and C−B interface in both Au|4-ZBNNR/ZGNR|Au and Au|4-ZGNR/ZBNNR|Au. Thus, only the C−B interface of hybrid systems offers additional transport channels in systems of Au|hybrid nanoribbons|Au. The potential barrier between Au and hybrid structures is the main reason of the lower enhancement of transmission conductance of Au|hybrid nanoribbons|Au than that of hybrid systems with pristine electrodes.

To realize the domain proposed by Semenoff et al.,[19] the substituted nanoribbons are located in the middle of either ZGNRs or ZBNNRs. To show the effect of substitution position on the transport properties of hybrid systems, we calculate the transmission conductance of 4-ZGNR/ZBNNR and 4-ZBNNR/ZGNR with different substitution positions (see Supporting Information Figure S2). The transmission platforms of $3G_0$ of 4-ZBNNR/ZGNR separate each other when the width of the ZGNR at either side is less than 3 zigzag chains. Such separation mainly derives from the coupling between B (N) atoms at the interface and edge C atoms. However, one platform of $3G_0$ remains around the Fermi level introduced by the coupling between B (N) and C atoms at the interface because of the additional band at each side of the Fermi level (see Supporting Information Figure S3). It indicates that the enhancement of the

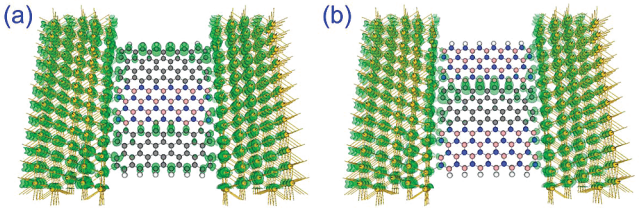

Figure 6. LDOS in the real space at the Fermi level of Au|4-ZBNNR/ZGNR|Au (a) and Au|4-ZGNR/ZBNNR|Au (b). The green shadows represent the distribution of LDOS. The white, pink, gray, blue, and golden balls denote the hydrogen, boron, carbon, nitrogen, and gold atoms, respectively.

transport properties of 4-ZBNNR/ZGNR compared with those of the pristine ZGNR is only slightly sensitive to the substitution position. The $2G_0$ transmission platform remains in 4-ZGNR/ZBNNR for different substitution positions, which means the enhancement of its transport properties compared with those of the pristine ZBNNR is independent of the substitution position. Therefore, the enhancement of transport properties of our proposed hybrid systems is only slightly sensitive to the substitution position.

To the end, it is worthy of noting that the hybrid structures used in our prototypic devices have not been achieved in experiments so far. However, some hybrid graphene and boron nitride structures, such as atomic layers of hybridized boron nitride and graphene domains, have been prepared in experiments recently.[28] Moreover, GNRs and BNNRs can be formed by unzipping the carbon nanotubes and boron nitride nanoribbons by plasma etching, respectively.[29,30] The well-ordered hybrid systems might be fabricated by self-assembly growth upon the template of unzipped CNTs and BNNTs or cutting from phase-separated atomic layers of hybridized boron nitride and graphene using lithographic technology. We look forward to the synthesis of hybrid ZGNRs−ZBNNRs and their based devices in experiments in the future to confirm our theoretical prediction.

CONCLUSION

In summary, we have studied the transport properties of hybrid ZGNRs−ZBNNRs systems. The strong coupling between C and B (N) atoms at the interface of hybrid systems effectively mixes their π orbitals and induces a pair of bonding and antibonding bands around the Fermi level, which induces the $3G_0$ platform and $2G_0$ peak at each side of the Fermi level in the transmission spectrum of ZGNR-based and ZBNNR-based hybrid systems, respectively. The platforms overlap at the Fermi level as the ribbon width of substituted nanoribbons increases and highly enhance the transport properties of hybrid structures. The transport enhancement remains in devices of hybrid nanoribbons combined with gold electrodes, and the currents of such devices are improved compared with those of pristine ones due to the additional transport channels originated from C−B interfaces. In view of the high transmission conductance around the Fermi level of hybrid systems, it is expected to be an effective way to modulate the transport properties of GNRs and BNNRs.

ASSOCIATED CONTENT

Supporting Information. Transport properties of Au|ZGNR|Au with different lengths of nanoribbons and transport

properties of 4-ZBNNR/ZGNR (4-ZGNR/ZBNNR) with different substitution positions. This material is available free of charge via the Internet at http://pubs.acs.org.

AUTHOR INFORMATION

Corresponding Author
*E-mail: lzsun@xtu.edu.cn; jxzhong@xtu.edu.cn.

ACKNOWLEDGMENT

This work was supported by the National Natural Science Foundation of China (Grant Nos. 10874143 and 10774127), the Specialized Research Fund for the Doctoral Program of Higher Education (Grant Nos. 20070530008 and 200805300003), the Cultivation Fund of the Key Scientific and Technical Innovation Project, the Ministry of Education of China (Grant No. 708068), the Scientific Research Fund of Hunan Provincial Education Department (Grant No. 10K065), and the Hunan Provincial Innovation Foundation for Postgraduate (Grant No. CX2010B266).

REFERENCES

(1) Novoselov, K. S.; Geim, A. K.; Morozov, S. V.; Jiang, D.; Zhang, Y.; Dubonos, S. V.; Grig- orieva, I. V.; Firsov, A. A. *Science* **2004**, *306*, 666–669.
(2) Novoselov, K. S.; Geim, A. K.; Morozov, S. V.; Jiang, D.; Katsnelson, M. I.; Grigorieva, I. V.; Dubonos, S. V.; Firsov, A. A. *Nature* **2005**, *438*, 197–200.
(3) Son, Y.-W.; Cohen, M. L.; Louie, S. G. *Phys. Rev. Lett.* **2006**, *97*, 216803.
(4) Wang, X.; Li, X.; Zhang, L.; Yoon, Y.; Weber, P. K.; Wang, H.; Guo, J.; Dai, H. *Science* **2009**, *324*, 768–771.
(5) Jin, C.; Lin, F.; Suenaga, K.; Iijima, S. *Phys. Rev. Lett.* **2009**, *102*, 195505.
(6) Pacilé, D.; Meyer, J. C.; Girit, Ç. Ö.; Zettl, A. *Appl. Phys. Lett.* **2008**, *92*, 133107.
(7) Han, W.-Q.; Wu, L.; Zhu, Y.; Watanabe, K.; Taniguchi, T. *Appl. Phys. Lett.* **2008**, *93*, 223103.
(8) Park, C.-H.; Louie, S. G. *Nano Lett.* **2008**, *8*, 2200–2203.
(9) Zhang, Z.; Guo, W. *Phys. Rev. B* **2008**, *77*, 075403.
(10) Gao, X.; Zhou, Z.; Zhao, Y.; Nagase, S.; Zhang, S. B.; Chen, Z. *J. Phys. Chem. C* **2008**, *112*, 12677–12682.
(11) Chen, W.; Li, Y.; Yu, G.; Zhou, Z.; Chen, Z. *J. Chem. Theory Comput.* **2009**, *5*, 3088–3095.
(12) Chen, W.; Li, Y.; Yu, G.; Li, C.-Z.; Zhang, S. B.; Zhou, Z.; Chen, Z. *J. Am. Chem. Soc.* **2010**, *132*, 1699–1705.
(13) Li, Y.; Zhou, Z.; Shen, P.; Chen, Z. *J. Phys. Chem. C* **2009**, *113*, 15043–15045.
(14) Du, A.; Chen, Y.; Zhu, Z.; Lu, G.; Smith, S. C. *J. Am. Chem. Soc.* **2009**, *131*, 1682–1683.
(15) Ding, Y.; Wang, Y.; Ni, J. *Appl. Phys. Lett.* **2009**, *95*, 123105.
(16) Dutta, S.; Manna, A. K.; Pati, S. K. *Phys. Rev. Lett.* **2009**, *102*, 096601.
(17) Kan, E.-J.; Wu, X.; Li, Z.; Zeng, X. C.; Yang, J.; Hou, J. G. *J. Chem. Phys.* **2008**, *129*, 084712.
(18) Pruneda, J. M. *Phys. Rev. B* **2010**, *81*, 161409.
(19) Semenoff, G. W.; Semenoff, V.; Zhou, F. *Phys. Rev. Lett.* **2008**, *101*, 087204.
(20) Kresse, G.; Furthmüller, J. *Phys. Rev. B* **1996**, *54*, 11169–11186.
(21) Kresse, G.; Furthmüller, J. *Comput. Mater. Sci.* **1996**, *6*, 15–50.
(22) Perdew, J. P.; Burke, K.; Ernzerhof, M. *Phys. Rev. Lett.* **1996**, *77*, 3865–3868.
(23) Brandbyge, M.; Mozos, J.-L.; Ordejón, P.; Taylor, J.; Stokbro, K. *Phys. Rev. B* **2002**, *65*, 165401.
(24) Li, Z.; Qian, H.; Wu, J.; Gu, B.-L.; Duan, W. *Phys. Rev. Lett.* **2008**, *100*, 206802.
(25) Mermin, N. D.; Wagner, H. *Phys. Rev. Lett.* **1966**, *17*, 1133–1136.
(26) Hod, O.; Barone, V.; Peralta, J. E.; Scuseria, G. E. *Nano Lett.* **2007**, *7*, 2295–2299.
(27) http://www.quantumwise.com/documents/tutorials/latest/BasicGrapheneTutorial/index.html/chap.zigzag_transport.html#chap.zigzag_transport.perfect (accessed May 5, 2011).
(28) Ci, L.; Song, L.; Jin, C.; Jariwala, D.; Wu, D.; Li, Y.; Srivastava, A.; Wang, Z. F.; Storr, K.; Balicas, L.; Liu, F.; Ajayan, P. M. *Nat. Mater.* **2010**, *9*, 430–435.
(29) Jiao, L.; Zhang, L.; Wang, X.; Diankov, G.; Dai, H. *Nature* **2009**, *458*, 877–880.
(30) Zeng, H.; Zhi, C.; Zhang, Z.; Wei, X.; Wang, X.; Guo, W.; Bando, Y.; Golberg, D. *Nano Lett.* **2010**, *10*, 5049–5055.